Homogeneous interface-type resistance switching in $Au/La_{0.67}Ca_{0.33}MnO_3/SrTiO_3/F:SnO_2$ heterojunction memories*

Zhang Ting(张 婷), Ding Ling-Hong(丁玲红), and Zhang Wei-Feng(张伟风)†

Key Laboratory of Photovoltaic Materials of Henan Province, School of Physics and Electronics, He'nan University, Kaifeng 475004, *China*

(Received 8 September 2011; revised manuscript received 19 October 2011)

$La_{0.67}Ca_{0.33}MnO_3$ thin films are fabricated on fluorine-doped tin oxide conducting glass substrates by a pulsed laser deposition technique with $SrTiO_3$ used as a buffer layer. The current-voltage characteristics of the heterojunctions exhibit an asymmetric and resistance switching behaviour. A homogeneous interface-type conduction mechanism is also reported using impedance spectroscopy. The spatial homogeneity of the charge carrier distribution leads to field-induced potential-barrier change at the Au-$La_{0.67}Ca_{0.33}MnO_3$ interface and a concomitant resistance switching effect. The ratio of the high resistance state to the low resistance state is found to be as high as 1.3×10^4% by simulating the AC electric field. This colossal resistance switching effect will greatly improve the signal-to-noise ratio in nonvolatile memory applications.

Keywords: $La_{0.67}Ca_{0.33}MnO_3$ thin films, resistance switching, impedance spectroscopy, metal–oxide interface

PACS: 73.40.–c, 73.40.Rw, 73.50.Fq, 72.20.–i **DOI:** 10.1088/1674-1056/21/4/047301

1. Introduction

Recently, resistance random access memory (RRAM) has aroused great interest due to its excellent scalability, simple structure, fast switching speed, long retention time, and nondestructive readout.[1–8] Among all materials devices, electric-pulse-induced resistance (EPIR) switching based on perovskite-type manganese $Re_{1-x}A_xMnO_3$ (Re = rare earth ions, A = alkaline ions, x = 0.3–0.7) has attracted considerable attention for potential applications in next-generation nonvolatile memories.[2–8] To explain the intriguing switching effect in these manganese materials, a few qualitative models have been proposed that emphasize different aspects: electric field-induced defect migration,[9] phase separation,[10] tunneling across interfacial domains,[11] control of the Shottky barrier's height,[12] etc. However, the accepted mechanism behind the physical effect remains elusive. At present, there are two competing explanations of resistance switching, i.e. bulk effect and interface effect. For instance, bulk charge ordering in $Pr_{0.7}Ca_{0.3}MnO_3$ has been suggested, but this creates an apparent conflict with both the spatial symmetry and the reported bulk properties.[13] Although an interface model has been proposed involving either lattice defects or carrier concentration, the exact nature of this interface remains vague.[14] To clarify how and where resistance switching occurs, a convenient and effective test technique that could investigate the carrier transport modes in semiconductors and insulators must be obtained. Complex-impedance-plane plots are very popular because the shape of the locus of points yields an insight into the possible mechanism or governing phenomenon. The bulk- and interface-related properties could be effectively separated by using impedance spectroscopy.[15]

In this work, we study the carrier transport mechanism in $La_{0.67}Ca_{0.33}MnO_3$ (LCMO) thin films mainly using the measurements of impedance spectrum characteristics. Here, $SrTiO_3$ (STO) is used as the buffer layer because of its low mismatch of the lattice constant between LCMO ($a_{\rm bulk}$ = 0.3864 nm and $c_{\rm bulk}$ = 0.3875 nm) and STO ($c_{\rm bulk}$ = 0.3905 nm). The purpose of the present work is to investigate the qualitative difference of the Nyquist diagram (Cole–Cole plot) in the Au/LCMnO/STO/F:SnO_2(FTO) heterojunctions that have been experimentally ob-

*Project supported by the National Natural Science Foundation of China (Grant No. 60976016), the Program for Innovative Research Team in Science and Technology in University of Henan Province (IRTSTHN), China (Grant No. 2012IRTSTHN004), and the Research Program of Henan University, China (Grant No. SBGJ090503).

†Corresponding author. E-mail: wfzhang@henu.edu.cn

© 2012 Chinese Physical Society and IOP Publishing Ltd

served so far, and to correlate the Cole–Cole plot type with a certain physical mechanism of resistance switching.

2. Experimental details

The ceramic targets for STO and LCMO were prepared by a standard solid state reaction method using $SrCO_3$, TiO_2, La_2O_3, $CaCO_3$, and MnO_2 as the raw materials. Using an STO buffer, an LCMO/FTO heterojunction was grown in a pulsed laser deposion (PLD) system with an operation wavelength of KrF (λ = 248 nm, repetition rate = 5 Hz, a single pulse power = 300 mJ). FTO conducting glass was adopted as a bottom electrode for its lower sheet resistance (15.87 $\Omega/\Box$) because its resistivity and surface have a rather small change, with the annealing temperature increasing up to 750 °C, and it is suited for the practical application of resistance switching. Firstly, approximately 40 nm STO was deposited on a chemically cleaned FTO substrate. Secondly, a 400-nm thick LCMO film was grown. The deposition was carried out at 700 °C under an O_2 partial pressure of 20 Pa. Finally, Au top electrodes with a diameter of 200 μm were deposited by DC sputtering with a metal shadow mask.

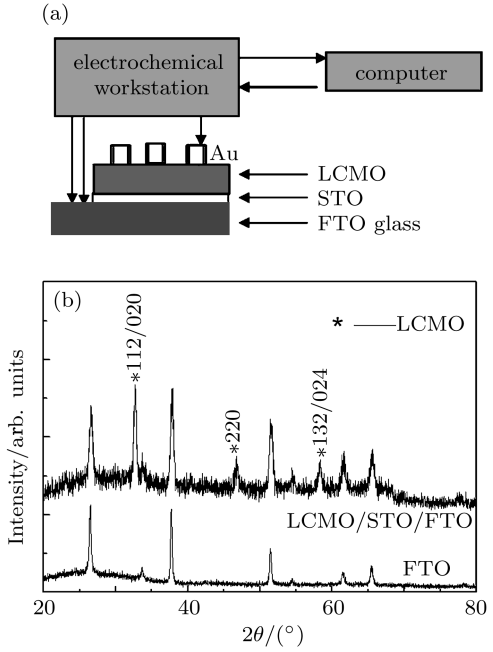


Fig. 1. (a) Schematic diagram of the I–V measurement system. (b) XRD patterns of the LCMO thin films on STO/FTO.

The film structures were determined on a DX-2500 X-ray diffractometer at a range of 20°–80° (2θ), employing Cu Ka radiation (1.542 Å, 1 Å = 0.1 nm). Cyclic voltammetry and AC impedance measurements were performed using a CHI600B electrochemical workstation (Chenhua instruments Inc., China). All the electrochemical measurements were carried out using a three-electrode system with FTO used as a reference electrode and counter electrode, and Au as the working electrode. The data were recorded using a computer controlled program. Figure 1(a) shows a schematic diagram of the measurement setup of the electric-pulse-induced resistance (EPIR) change effect.

3. Results and discussion

The obtained XRD patterns of the LCMO/STO thin films on FTO are shown in Fig. 1(b). All the diffraction peaks can be indexed to LCMO and SnO_2 (from FTO substrates), indicating that the films are of single phase without any impurity.

The current–voltage (I–V) characteristics of Au/LCMO/STO/FTO under the voltage sweep $0 \rightarrow V_{\max} \rightarrow 0 \rightarrow -V_{\max} \rightarrow 0$ are shown in Fig. 2. Here, positive bias is defined as electric current flowing from Au to FTO. It can be seen that the curves exhibit nonlinear and asymmetry behaviours, along with a clear hysteresis at negative bias. Two stable resistance states are obtained by voltage sweeping. When the applied voltage bias increases from 0 to $V_{\max}$, the slope of the I–V curve cannot be observed obviously and the

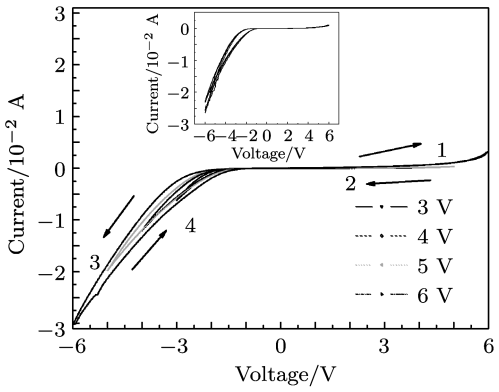


Fig. 2. The current–voltage characteristics of Au/LCMO/STO/FTO in different bias voltage ranges. The inset indicates the 15 consecutive measurements performed with a 0.3 V/s scanning rate.

device is in a high resistance state (HRS). It remains in a HRS by a change of the scanning direction, until the applied voltage preponderates over a negative numerical value. The current across the sample increases suddenly from this point and the device is switched into

a low resistance state (LRS). After that, the device remains in an LRS as the voltage returns to zero and switches again to HRS. A similar phenomenon has also been observed in perovskite oxide,[16] sulfide,[17] and organic polymeric thin films.[18] Furthermore, the hysteresis window becomes bigger and bigger with the increase in voltage range, which provides the possibility of the existence of multilevel resistance switching. The 15 consecutive measurements were performed with a 0.05 V/s scanning rate between 6 V and −6 V. The device shows a satisfactory reproducibility, as shown in the inset of Fig. 2.

The domain model may be used to simulate quite divergent DC I–V characteristics by adjusting the fitting parameters,[19] and the AC impedance is expected to survey the resistance switching.[15] The impedance spectra of the sample in a frequency range of 10^0–10^5 Hz were measured at 0 V dc bias with a voltage oscillation amplitude of 5 mV. The result is shown in Fig. 3(a). Intentionally, before the impedance spectral

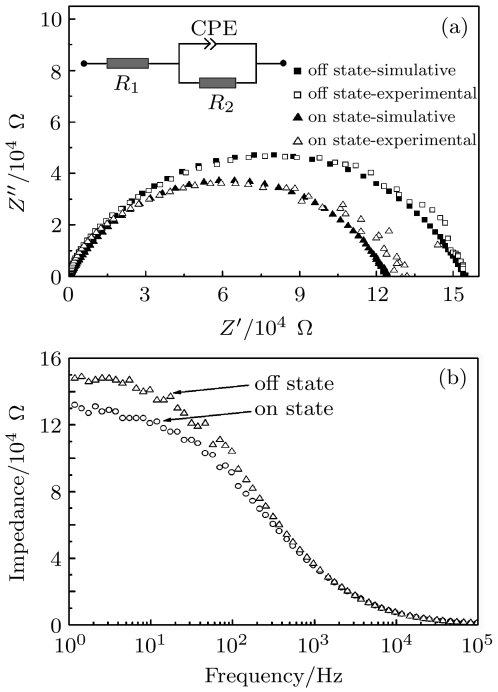


Fig. 3. (a) Measured impedance spectra of the LCMO memory device (open symbols) and simulated impedance spectra (solid symbols), with the inset showing the corresponding equivalent circuit model. (b) The frequency dependence of the impedance in the on and off state.

measurement, the Au/LCMO/STO/FTO assembled circuit was first driven by a continuous sweeping voltage to the switch-on state and then terminated at the switch-off state. It should be noted that the arc depression is not negligible with regard to the real impedance axis, as shown in Fig. 3(a), where the centre of a simulated impedance arc is located below the real axis of a complex plane. Depression analysis at Nyquist plots ($-Z_{\rm imaginary}$ versus $Z_{\rm real}$) provides the information concerning homogeneity in the electrical/dielectric origin governing the corresponding impedance responses.[20] A computer simulation of the process enabled us to create the corresponding equivalent circuit with the help of the Zview-2 program. The equivalent circuit in different electronic states can be described by a resistor $R_{\rm e}$ in series with the parallel combination of $R_{\rm t}$ and a constant phase element (CPE). Such a CPE is often used in a model in the place of a capacitor to compensate for non-homogeneity in the system to take into account the irregularity of the surface. For example, a rough or porous surface can cause a double-layer capacitance to appear as a constant phase element. In the present work, the non-homogeneity could arise from the surface heterogeneities such as grain boundaries, crystal faces on a polycrystalline electrode, or other variations in surface property. For the equivalent circuit plotted in Fig. 3(a), the impedance is given by[21]

$$Z(\omega) = R_{\rm e} + \frac{R_{\rm t}}{1 + ({\rm j}\omega)^{P_{\rm CPE}} T_{\rm CPE} R_{\rm t}}, \qquad (1)$$

where the $R_{\rm e}$ value depends only on the connection resistance, $R_{\rm t}$ is the charge transfer resistance, CPE represents the capacitive behaviour of the double layer replacing the ideal capacitance from the frequency angle and the diffusion behavior, $T_{\rm CPE}$ is the electrostatic capacitance (F), and $P_{\rm CPE}$ is the index (dimensionless) indicating a degree of deviation from a certain state. For low frequencies, the total resistance equals the sum of $R_{\rm e}$ and $R_{\rm t}$. With increasing frequency, the impedance of the capacitance reduces. At very high frequencies, the impedance of the capacitance is almost zero and therefore the capacitance acts as a short circuit. Thus, $R_{\rm e}$ is directly measured at high frequencies. The high-frequency component generally corresponds to true bulk contributions, the intermediate frequency term is ascribed to the resistive grain boundaries, and the low-frequency term corresponds to electrode interface contributions.[22] By comparing the two semicircular arcs of the HRS and LRS in Fig. 3(a), no significant difference can be observed in the high-frequency region originating from the LCMO bulk contribution. However, the semicircular arc of the HRS originating from the interface is much larger than that of LRS. These results show that the resistance change in the LCMO heterojunction would originate from the change in the interfacial

resistance. A so-called homogeneous interface-type conduction mechanism[23] may play an important role in our device, in which the change in resistance is attributed to the field-induced change of the potential-barrier at the interface.

In Fig. 3(a), the impedance spectral characteristics of the on and off states each exhibit a high resistive value. A high density of defects exists at each of the Au/LCMO, LCMO/STO, and STO/FTO interfaces, where the high density of surface states induced by the defects may cause a large degree of band bending and then influence the validity of the metal/semiconductor contact rule in the Au/LCMO/STO/FTO heterojunctions.

Detailed circuit parameters of the simulant plots of the on and off electronic states are summarized in Table 1. Because the high-frequency range is corresponding to the resistance from the bulk portion,[24] this is similar to the scale of resistance obtained with DC I–V measurements. The change in bulk-related $R_{\rm e}$ is not visible, while $R_{\rm t}$ represents the charge transfer at the electrode–semiconductor interface which changes remarkably. It indicates a significantly changed interface resistance existing in different electronic states. In addition, the switching behaviour could be explained in terms of the interfacial response originating from the Au/LCMO contacts.[20]

Table 1. Summary of the equivalent circuit parameters obtained using the impedance spectra of Fig. 3(a) in the on and off states.

	$R_{\rm e}/\Omega$	$T_{\rm CPE}$/F	$P_{\rm CPE}$	$R_{\rm t}/\Omega$
Off state	274	3.6069×10^{-8}	0.69824	149410
On state	272	3.6067×10^{-8}	0.68824	124110

One disadvantage of the complex-impedance-plane format is that the frequency dependence is obscured. Frequency is generally presented on a logarithmic scale to reveal the important behaviour seen at lower frequencies. Therefore, the impedance associated with frequency plots is depicted in Fig. 3(b). The measured impedance is expected to be ω-dependent. Interestingly, the impedance information obtained during the off state is similar to that obtained during the on state. The AC sweeping shows a gradual decrease in impedance unlike the rapid changes in the I–V characteristics. Once the device is in the high impedance state, it can be switched to higher conductive states by applying different frequencies, which is also considered to be a precursor sign of multi-level resistance switching.

It has been found that the interface resistance between the electrode and LCMO is much larger than the intrinsic resistance of LCMO polycrystalline ceramics (0.01 $\Omega \cdot$cm–0.2 $\Omega \cdot$cm), and it is believed that the transport properties are dominated by the interface. The colossal electro-resistance caused by low current in the perovskite manganese film has been reported and the carrier transport in the system is often interpreted in terms of interface effect. Some researchers have attributed the effect to the film/electrode interface, in which Schottky barriers with trapped charges and space-charge-limited current are involved.[25,26] In our case, the devices with LCMO films and metal electrodes of similar work functions have shown drastically different I–V characteristics and resistance switching phenomena. These suggest that carrier transport at interfaces cannot simply be explained by the Schottky barrier effect. Recently, high resolution transmission electron microscopy has confirmed the existence of a metal–oxide layer between the metal electrode and the perovskite film.[27,28] It was argued that the resistance switching effect is due to the formation and dissociation of such an interfacial metal–oxide layer. Nevertheless, the formation of a metal–oxide layer at the Au/LCMO interface could not be used to interpret the present system due to the good stability of Au. It has been discussed that the strong electric field develops at the highly resistive dielectric-electrode interface, leading to a spatially inhomogeneous oxygen vacancy distribution and a concomitant resistive switching effect.[29] For a better understanding of the charge carrier transport mechanism, the typical Nyquist impedance responses of the Au/LCMO/STO/FTO heterojunctions at several applied DC biases are shown in Fig. 4(a). Interestingly, depressed semicircles appear in impedance spectra by applying different DC biases. Significantly, with the increase in the DC bias, the large semicircle shrinks, which is a typical characteristic of a Faradic charge-transfer and reactions among species at the interface, such as Mn ions (Mn^{3+} and Mn^{4+}), electrons, oxygen vacancies and oxygen atoms. The predominant charge (electrons and Mn ions) and mass transfer (Mn^{3+} and Mn^{4+} ions, oxygen atoms and oxygen ions) may occur at this interface due to the local solid electrochemical reaction. The presence of the interface (junction) between the Au and LCMO might behave like a potential barrier, and charge carriers are accumulated at the junction. At a low bias voltage, the electric field is not sufficient for charge carriers to overcome the barrier. Therefore, the conductivity of the film is not affected. As the applied bias voltage increases, charge carriers gain enough energy from the applied electric field to cross the junction at the interface,

hence the conductivity increases. For example, resistive switching relies on the attraction of oxygen vacancies into the Au/LCMO interface and a corresponding decrease in the Schottky-like interface barrier for negative voltages (LRS), and a repulsion of oxygen vacancies with a corresponding recovery of that barrier for positive voltages (HRS). So the conductivity could be attributed to the accumulation and diffusion of charge carriers at the interface, and it hints at a homogeneous interface-type conduction mechanism.

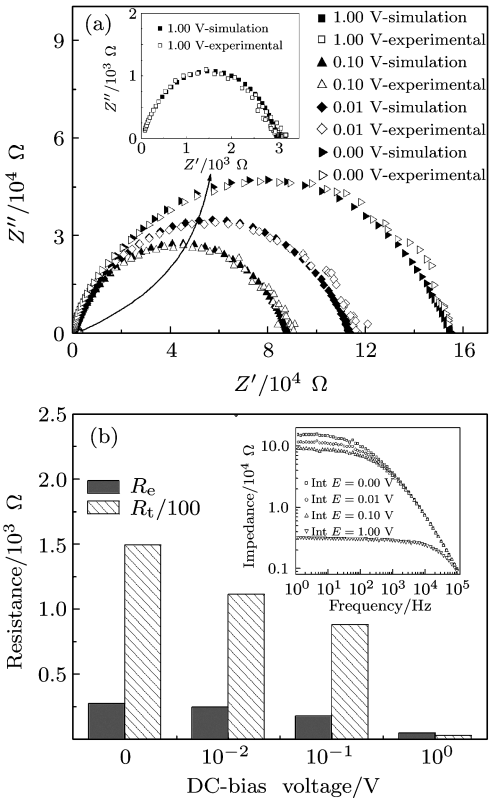


Fig. 4. (a) DC-bias-dependent impedance of the LCMO memory device (open symbols), and simulated impedance spectra (solid symbols). (b) Histogram of R_e and R_t corresponding to DC-bias-dependent impedance spectra. The inset indicates the frequency dependence of the impedance spectra of Au/LCMO/STO/FTO subject to different DC bias voltages.

As indicated in Table 2, the data validation proves that the experimental results fit reasonably and are in good agreement with the proposed circuit model. The DC-bias-dependent circuit parameters R_e and R_t in Table 2 are displayed in Fig. 4(b). It can be clearly observed that R_t represents the charge transfer at the electrode–semiconductor interface and changes remarkably with different DC bias. The impedances associated with frequency plots by applying different DC-bias voltages are depicted in the inset of Fig. 4(b). Interestingly, the different bias sweepings show an obvious impedance change in the low-frequency region. These results show that a proper DC bias can significantly improve the resistance switching behaviour. Although we discover that the hysteretic behaviour mainly originates from the Au/LCMO interface, as discussed above, the exact effect of a heterojunction composed of two resistance states could not be specified by applying different voltages from the present results alone. Further studies, such as chemical and structural analyses at the interface, should be performed in detail later on.

Table 2. Summary of the equivalent circuit parameters obtained using the impedance spectra of Fig. 4(a).

Bias voltage/V	R_e/Ω	$T_{CPE}/10^{-8}$ F	P_{CPE}	R_t/Ω
0.00	274	3.607	0.69824	149410
0.01	247	3.132	0.70201	111540
0.10	180	3.199	0.71204	88007
1.00	46	3.005	0.79423	3005

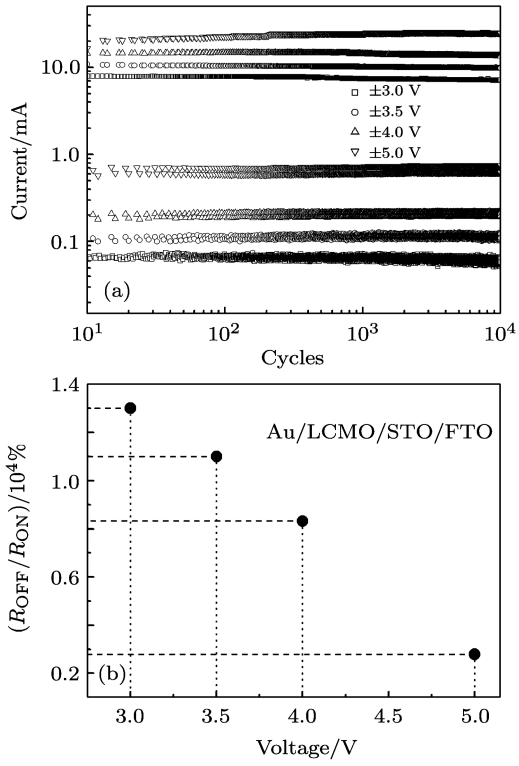


Fig. 5. (a) Multilevel switching behaviours and the endurance of the Au/LCMO/STO/FTO heterostructures at different applied bias voltages. (b) The ratio of R_{off}/R_{on} as a function of bias voltage.

Figure 5(a) demonstrates the multilevel resistance switching of the LCMO thin film device. Different high-resistance states are obtained by applying electric-pulse voltages of 3, 3.5, 4, and 5 V with a pulse width of 0.002 s, and the changed low-resistance states are observed by applying electric-pulse voltages of −3, −3.5, −4, and −5 V with a pulse width of

0.002 s. Over 1×10^4 switching cycles, the two states triggered by positive and negative electric pulses, are almost unchanged. This multilevel resistance switching feature can be used as the high-density storage, and the endurance characteristic indicates that the device becomes negligibly degraded. The values of the switching ratio $R_{\rm off}/R_{\rm on}$ performed at different electric-pulse voltages are denoted in Fig. 5(b). When ± 5 V with a pulse width of 0.002 s electric-pulse voltages are applied, the ratio of the heterojunctions can reach 1.3×10^4%. This will greatly improve the signal-to-noise ratio for nonvolatile memory applications.

4. Conclusions

We report on the current-induced switching effect in Au/LCMO/FTO heterojunctions using STO as a buffer layer. A distinctive feature is that the transport behaviour of the device is sensitive to the external field, and a switching of the resistance between two definite resistive states can be induced by electric pulses of different polarities. The use of impedance spectroscopy allows for the separation between the interfacial effects and the bulk responses. A homogeneous interface-type conduction effect is discussed in the metal/LCMO junction. Charge and mass transfers may occur at this interface due to the local solid electrochemical reaction, and the change in resistance is attributed to the field-induced change in the potential barrier at the Au-$La_{0.67}Ca_{0.33}MnO_3$ interface. Several resistance states are obtained by modulating the electric-pulse voltage. It is expected that the resistance switching behaviour observed in this work can make it possible to integrate non-volatile multilevel memory devices on glass substrates.

References

[1] Li Y T, Long S B, Lü H B, Liu Q, Wang Q, Wang Y, Zhang S, Lian W T, Liu S and Liu M 2011 *Chin. Phys.* B **20** 017305

[2] Meng Y, Zhang P J, Liu Z Y, Liao Z L, Pan X Y, Liang X J, Zhao H W and Chen D M 2010 *Chin. Phys.* B **19** 037304

[3] Sheng Z G, Gao J and Sun Y P 2009 *Phys. Rev.* B **79** 014433

[4] Yasuhara R, Yamamoto T, Ohkubo I, Kumigashira H and Oshima M 2010 *Appl. Phys. Lett.* **97** 132111

[5] Liu X J, Kuyyadi Biju P, Mostafa Bourim E, Park S, Lee W, Lee D, Seo K and Hwang H 2011 *Electrochem. Solid-State Lett.* **14** H9

[6] Lee W, Jo G, Lee S, Park J, Jo M, Lee J, Jung S, Kim S, Shin J, Park S, Lee T and Hwang H 2011 *Appl. Phys. Lett.* **98** 032105

[7] Ouyang J Y, Chu C W, Szmanda C R, Ma L P and Yang Y 2004 *Nature Mater.* **3** 918

[8] Zhang T, Su Z H, Chen H J, Ding L H and Zhang W F 2008 *Appl. Phys. Lett.* **93** 172104

[9] Nian Y B, Strozier J, Wu N J, Chen X and Ignatiev A 2007 *Phys. Rev. Lett.* **98** 146403

[10] Tulina N A, Zver'kov S A, Mukovskii Y M and Shulyatev D A 2001 *Europhys. Lett.* **56** 836

[11] Rozenberg M J, Inoue I H and Sánchez M J 2004 *Phys. Rev. Lett.* **92** 178302

[12] Jeong D S, Schroeder H and Waser R 2009 *Phys. Rev.* B **79** 195317

[13] Liu S Q, Wu N J and Ignatiev A 2000 *Appl. Phys. Lett.* **76** 2749

[14] Tsui S, Baikalov A, Cmaidalka J, Sun Y Y, Wang Y Q, Xue Y Y, Chu C W, Chen L and Jacobson A J 2004 *Appl. Phys. Lett.* **85** 317

[15] Zhang T, Zhang X A, Ding L H and Zhang W F 2009 *Nanoscale Res. Lett.* **4** 1309

[16] Lau H K, Leung C W, Hu W H and Chan P K L 2009 *J. Appl. Phys.* **106** 014504

[17] Morales-Masis M, van der Molen S J, Fu W T, Hesselberth M B and van Ruitenbeek J M 2009 *Nanotechnology* **20** 095710

[18] Yang Y, Ouyang J, Ma L, Tseng R J H and Chu C W 2006 *Adv. Funct. Mater.* **16** 1001

[19] Tsui S, Wang Y Q, Xue Y Y and Chu C W 2006 *Appl. Phys. Lett.* **89** 123502

[20] You Y H, So B S, Hwang J H, Cho W, Lee S S, Chung T M, Kim C G and An K S 2006 *Appl. Phys. Lett.* **89** 222105

[21] Orazem M E and Tribollet B 2008 *Electrochemical Impedance Spectroscopy* (New Jersey: The Electrochemical Society) p. 311

[22] Abrantesa J C C, Labrinchab J A and Fradeb J R 2000 *Materials Research Bulletin* **35** 727

[23] Muenstermann R, Menke T, Dittmann R and Waser R 2010 *Adv. Mater.* **22** 4819

[24] Liang C H, Terabe K, Hasegawa T and Aono M 2007 *Nanotechnology* **18** 485202

[25] Sawa A, Fujii T, Kawasaki M and Tokura Y 2004 *Appl. Phys. Lett.* **85** 4073

[26] Tsubouchi K, Ohkubo I, Kumigashira H, Oshima M, Matsumoto Y, Itaka K, Ohnishi T, Lippmaa M and Koinuma H 2007 *Adv. Mater.* (Weinheim, Ger.) **19** 1711

[27] Li S L, Liao Z L, Li J, Gang J L and Zheng D N 2009 *J. Phys.* D **42** 045411

[28] Shono K, Kawano H, Yokota T and Gomi M 2008 *Appl. Phys. Express* **1** 055002

[29] Rozenberg M J, Sanchez M J, Weht R, Acha C, Gomez-Marlasca F and Levy P 2010 *Phys. Rev.* B **81** 115101